Geoscience Letters

RESEARCH LETTER

Open Access

The landslide source of the eastern Mediterranean tsunami on 6 February 2023 following the M_w 7.8 Kahramanmaraş (Türkiye) inland earthquake

Mohammad Heidarzadeh[1*], Aditya Riadi Gusman[2] and Iyan E. Mulia[3,4]

Abstract

This paper presents the first example of how to systematically identify the submarine landslide source of a tsunami using an innovative hybrid approach. This ground-breaking method is developed to resolve the puzzle around the source mechanism of the mysterious tsunami observed on 6th February 2023 in the Eastern Mediterranean Sea. The tsunami followed the two inland M_w 7.8 and M_w 7.5 Türkiye–Syria earthquakes, which occurred consequently with a 9 h interval on this day. The first earthquake (M_w 7.8) had an epicentral distance of 90 km from the nearest coast, which is closer than the second one (M_w 7.5) to the coast and yet its crustal deformation was almost entirely limited to inland. Therefore, the co-seismic surface displacement generated by the earthquake was ruled out as the source of the tsunami, confirmed by numerical modelling. Here, we hypothesized that the tsunami was most likely generated by a submarine landslide triggered by the earthquake. Analysis of tide gauge observations revealed that the waves arrived from 27 min to 48 min after the first earthquake (M_w 7.8) at different coastal locations, implying that the potential submarine landslide was triggered by the first earthquake (M_w 7.8). Backward tsunami travel time mapping using tide gauge observations guided us to constrain the area of the potential landslide. We approximated the dimensions of the landslide using spectral analysis of the tsunami observations. Consequently, an iterative trial-and-error approach was employed to confirm the landslide source of the tsunami by defining various informed alternative landslide scenarios and applying numerical modeling. Modelling showed that a submarine landslide can reproduce the tsunami observations reasonably well. It is located on a steep slope of the seafloor approximately 50 km from Arsuz. The submarine landslide is estimated to have caused a seafloor deformation measuring approximately 16 km in length and 4.0 km in width.

Keywords Mediterranean Sea, Türkiye, Kahramanmaraş earthquake, Tsunami, Landslide, Numerical modelling

*Correspondence:
Mohammad Heidarzadeh
mhk58@bath.ac.uk
Full list of author information is available at the end of the article

Introduction

The Türkiye–Syria border was struck by two large earthquakes (M_w 7.8 and M_w 7.5; Fig. 1) on 6th February 2023 within nine hours leaving a death toll of over 50,000 (International Medical Corps 2023). According to the United States Geological Survey (USGS), both events were the results of strike-slip faulting and occurred at shallow depths of 17.9 km and 10.0 km for the M_w 7.8 and M_w 7.5 events, respectively. The respective origin times were 01:17:35 UTC (for M_w 7.8) and 10:24:49 UTC (for M_w 7.5). These devastating earthquakes remind the tragedy generated by the 17th August 1999 Izmit earthquake (M_w 7.4) in northwestern Türkiye (Fig. 1) which killed over 17,000 people (Barka 1999; Yalciner et al. 1999; Ozalaybey et al. 2002).

The epicenters of the two recent 2023 earthquakes are located within a triple junction where three tectonic plates (the Anatolian, Arabian and African plates) meet (Fig. 1). Although theoretically triple junctions are thought to develop high levels of tectonic strains and stresses, the region had not experienced any earthquake larger than M 6.7 in the past 100 years. Possibly this is a reason that the recent M_w 7.8 and M_w 7.5 events came as surprises to the authorities and public and caused unprecedented damage and deaths.

A moderate-size tsunami was generated in the eastern Mediterranean Sea following the 6th February 2023 earthquakes, which was reported by local people, and was recorded on tide gauges (Fig. 2). As the earthquakes' epicenters were at least 90 km away from the coastline, it is not clear how the tsunami was generated. Normally, there are two possibilities: (1) Either the co-seismic crustal deformation was extended to the sea and generated the tsunami, or (2) the tsunami was generated by a coseismic submarine landslide or landslides triggered by the earthquakes. For the case of the 17th August 1999 Izmit Bay tsunami in Türkiye due to an inland M_w 7.4 earthquake (Fig. 1), it was shown by Tinti et al. (2006) that a submarine landslide contributed to the tsunami. Another example of a tsunami generated by an inland earthquake due to a coseismic submarine landslide is the tsunami of 24th September 2013 in the northwestern Indian Ocean following an inland M_w 7.7 earthquake in Pakistan (Heidarzadeh and Satake 2014). The recent February 2023 tsunami is the third tsunami to hit Türkiye in the past six years following the July 2017 and October 2020 tsunamis (Fig. 1) (Dogan et al. 2019, 2021; Heidarzadeh et al. 2017a, 2021). The region experienced historical tsunamis such as those in 749 AD and 1759 AD (Papadopoulos et al. 2014).

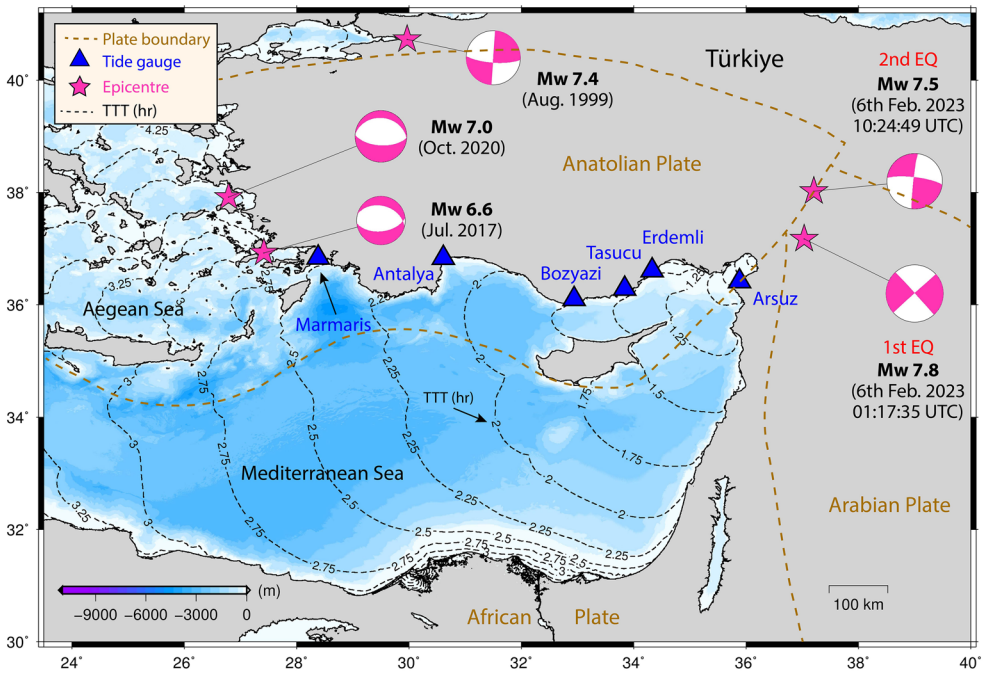

Fig. 1 Epicentral area of the two Türkiye–Syria earthquakes of 6th February 2023 (1st EQ and 2nd EQ). The tide gauges used in this study are shown as blue triangles, and the contours representing tsunami travel time (TTT) are shown as black dashed lines at 0.25 h (15 min) intervals. For TTT calculations, it is assumed that the earthquake source was the nearest water point to the epicenter of the 1st EQ. Brown dashed lines are approximations of adjacent plate boundaries. All epicenters and focal mechanisms are based on the USGS except for the event of 1999 which is from the solution made by the University of Tokyo (Japan)

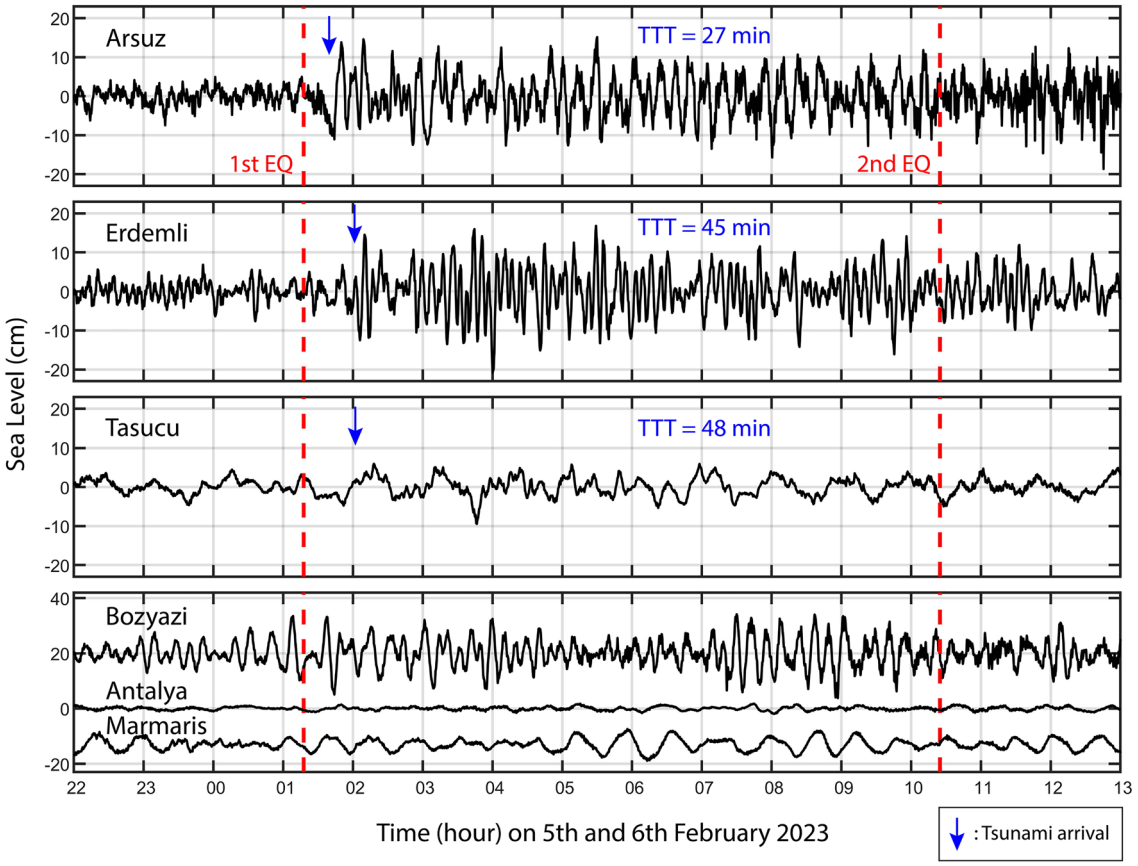

Fig. 2 The tide gauge records for six stations close to the epicenters of the 6th February 2023 Türkiye–Syria earthquakes (1st EQ and 2nd EQ). The blue arrows indicate tsunami arrivals in each station. Three stations (Bozyazi, Antalya, and Marmaris) do not show clear tsunami signals. TTT indicates tsunami travel time to each station. The red dashed vertical lines represent the origin times of the two earthquakes

Table 1 Information of tide gauge stations used in this research to study the 6th February 2023 Türkiye tsunami

Station name	Longitude (°)	Latitude (°)	Sampling interval (s)	Maximum tsunami amplitude (cm)	Tsunami travel time (min)
Arsuz	35.885	36.416	30	15.2 ± 2	27
Erdemli	34.328	36.611	30	16.8 ± 2	45
Tasucu	33.836	36.281	30	6.0 ± 3	48
Bozyazi	32.941	36.097	30	N/A	N/A
Antalya	30.613	36.836	30	N/A	N/A
Marmaris	28.385	36.838	30	N/A	N/A

Here "tsunami amplitude" refers to zero-to-crest amplitudes of the waves. N/A means a clear tsunami signal cannot be seen by visual inspections of the wave trends

For regional tsunami hazard assessment, it is critically important to identify which of the above two candidates (the earthquake, or a submarine landslide) was responsible for the February 2023 tsunami in the eastern Mediterranean Sea. Therefore, we developed this study with the objective of identifying the source of the tsunami. Here, we examine both possibilities (either co-seismic crustal deformation or co-seismic submarine landslides) through investigating tide gauge records of the tsunami and performing numerical simulations.

Data and methods

We collected and analyzed six tide gauge records of the tsunami (Table 1, Fig. 2). All records come with a sampling interval of 30 s and are provided by the Intergovernmental Oceanographic Commission's sea level station monitoring facility (http://www.ioc-sealevelmonitoring.org/map.php). The data underwent quality control to remove spikes. Tidal analysis was performed using the TIDALFIT package (Grinsted 2023) to calculate tide signals which were then removed from the original tide gauge data to obtain de-tided tsunami waveforms (Fig. 2). TIDALFIT is a Matlab package (MathWorks 2023) that employs ordinary least squares regression methods to fit tidal components to sea level data (e.g., Grinsted 2023; Heidarzadeh et al. 2017b, 2017c). It is noted that, according to Fig. 2, the tsunami was initiated by the first earthquake (M_w 7.8). It is challenging to know whether the second earthquake has generated any additional tsunami or not. Throughout this research, we exclusively focus on the tsunami generated by the first earthquake.

Spectral analyses in this study were conducted through Fourier and Wavelet analyses. For Fourier analysis, we applied an updated version of the Welch's (1967) power spectral density estimate presented by the function *pwelch(x)* in Matlab (MathWorks 2023) considering Hanning windows and 50% overlaps (Mulia et al. 2022; Wang et al. 2022; Heidarzadeh et al. 2017b; Heidarzadeh and Gusman 2021; Cheng et al. 2023a,b; Hu et al. 2023). Wavelet analysis was performed by applying the wavelet package of Torrence and Compo (1998) and considering the Morlet mother function.

The earthquake slip model is provided by the United States Geological Survey (USGS) (Fig. 3a). The corresponding coseismic crustal deformation is shown in Fig. 3b. The USGS fault model consists of three segments named S1, S2, and S3 discretized into subfaults with a size of approximately 8 km^2. Details on the fault slip modeling setup are available at the USGS website at https://earthquake.usgs.gov/earthquakes/eventpage/us6000jllz/finite-fault, with main fault parameters tabulated in Table 2.

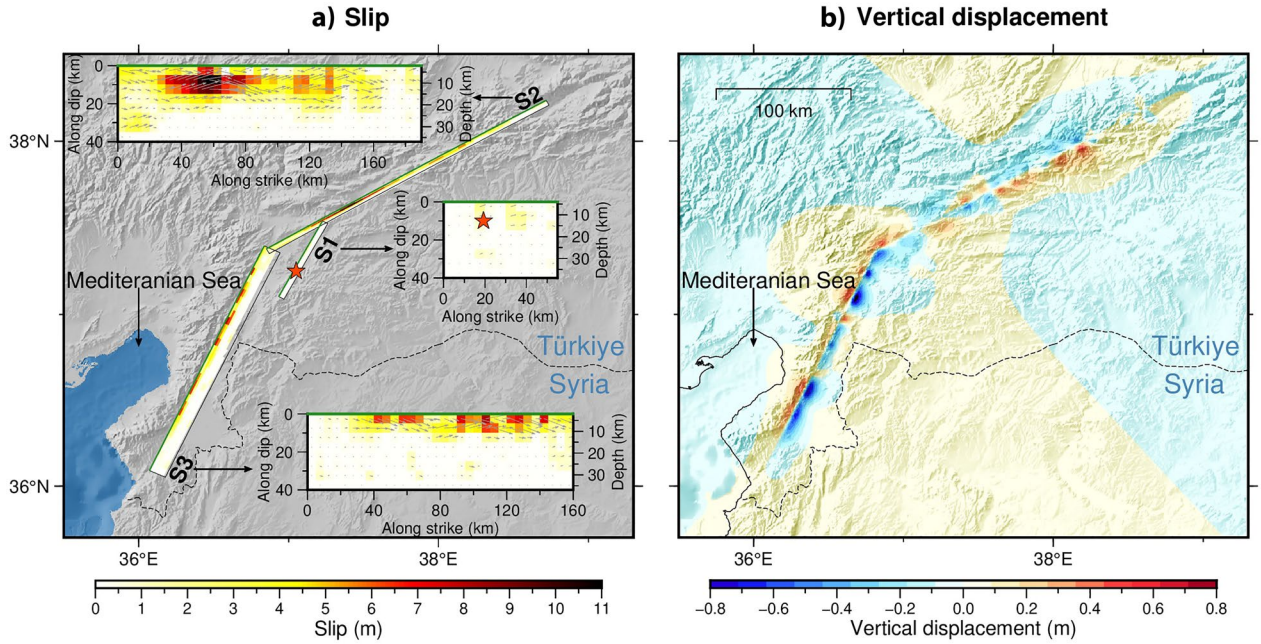

Fig. 3 The earthquake source model for the 6th February 2023 Türkiye–Syria M_w 7.8 earthquake developed by the USGS. The red stars indicate the epicenter. The model comprises three fault segments marked by S1, S2, and S3

Table 2 Fault parameters for the source model developed by the USGS for the 6th February 2023 M_w 7.8 Türkiye–Syria earthquake

Model developer	Segment	L (km)	W (km)	Top depth (km)	Strike (°)	Dip (°)	Rake (°)	Mean slip (m)
United States geological survey (USGS)	S1	55	40	4.0	28	85	340–379	0.2
	S2	190	40	2.0	60	85	339–379	1.9
	S3	160	40	1.9	25	75	339–379	1.0

We calculated the coseismic crustal deformation from the slip model using Okada's (1985) analytical formula, assuming an instantaneous crustal deformation. The effect of horizontal displacements on the tsunami genesis (Tanioka and Satake, 1996) was incorporated, which is necessary particularly for a strike-slip event. A maximum slip of 11 m occurred on S2, the largest segment, resulting in an uplift of up to 0.5 m and a subsidence of approximately 0.9 m inland (Fig. 3). The likely segment responsible for the tsunami was S3, being the closest to the sea. However, the average slip on this segment (i.e., S3) was only 1.0 m; hence it produced insignificant vertical displacements of less than 0.05 m on the seafloor.

The modelling package COMCOT (Cornell Multi-Grid Coupled Tsunami model) was used to simulate the tsunami from various source models evaluated in this study. COMCOT was originally developed at Cornell University (USA) in the 1990s (Liu et al. 1998; Wang 2008), and it has been under development at GNS Science, New Zealand since 2009 (Wang and Power 2011). In this study, a single bathymetric grid layer with a grid spacing of 15 arc-sec was used to simulate tsunami propagation and coastal amplifications. The Digital Elevation Model (DEM) data for the grid layer were extracted from the GEBCO (2022) (General Bathymetric Chart of the Oceans) bathymetric data which has an original resolution of 15 arc-second. We solved linear shallow water equations considering a time step of 0.1 s. Total simulation time was 4 h.

For landslide tsunami modelling, a Gaussian non-symmetric dipole initial source was considered as the input initial wave and thus a static tsunami initiation was applied following previous studies such as Synolakis et al. (2002), Satake and Tanioka (2003), Okal and Synolakis (2004), and Tappin et al. (2008). Although this method has been established as one of the reliable methods for modelling landslide tsunamis, its details yet to be developed. Among such details is the relationship between the dimension of the initial surface water displacement (L) and the length of the submarine landslide (b). This motivated us to conduct a few limited laboratory experiments, which were delivered through moving a submarine mass (a 20 cm long concrete block—see Fig. 4a) down a slope, with a slope angle of 47°, in a wave flume of the size 10 m (length) × 0.45 m (height) × 0.3 m (width). The water depth was 35 cm, the submergence depth was 5 cm (Fig. 4a), and the sliding mass was released at rest and moved down the slope under gravity. Results indicated the following relationship:

$$L \sim 2b \tag{1}$$

where L is the dimension of the initial surface water displacement, and b is the length of the submarine landslide. We acknowledge that Relationship (1) depends on the water depth, slope angle and the type of the material (either solid-block or granular), which are not examined in our limited physical experiments. Also, the slope angle of the physical experiment may be higher than the actual slope angle on the seafloor. Therefore, Relationship (1) is a preliminary result, and can be used only to give initial insights. It is challenging to know the duration of landslide occurrence due to limited data. However, we estimate it to be short (around 1–2 min) and speculate that landslides should have occurred at a high speed (approximately 20–40 m/s) because slow-moving landslides are not efficient towards tsunami generation. For example, by assuming an average velocity of 30 m/s and considering a travel distance of 2 km for the landslide, the duration of landslide occurrence will be 1.1 min.

Two pieces of information were gained from our physical experiments: (1) The initial wave generated by a submarine mass movement at the end of the wave generation has a dipole shape made of a negative (depression) phase shoreward and a positive (elevation) phase seaward (Fig. 4). And (2) The length of the initial surface water displacement is estimated at approximately twice of the length of the sliding mass (Relationship 1). Previously, other authors also considered dipole waves for modelling submarine landslide tsunamis (Synolakis et al. 2002; Satake and Tanioka 2003; Okal and Synolakis 2004; Watts et al. 2005; Grilli and Watts 2005; Tappin et al. 2008; Yalciner et al. 2014; Heidarzadeh et al. 2019). It is noted that the limited physical experiments conducted here were only used as a guide for developing alternative landslide source scenarios. Therefore, the limitations of the physical experiments do not have any impact on the outcomes of our research because the final source model are carefully tested through detailed numerical modeling on the actual bathymetry of the region and were validated through comparison with real tide gauge observations.

Characterization of the waves and estimating source lengths

Spectral and wavelet analyses are performed to characterize the waves (Fig. 5). For these analyses, we only considered two stations that registered most clear tsunami signals (Arsuz and Erdemli). Comparison of the tsunami spectra (blue-colored spectra) with the background ones (black-colored spectra) reveals peak tsunami periods. According to Fig. 5a, the peak tsunami periods are 5.4 min, 7 min, 12 min and 17 min in Arsuz, and they are 7 min, 13 min, and 21 min in Erdemli.

The tsunami source periods are normally those that occur in several stations and show large spectral energy differences with the background spectra or the peak periods that appear in spectral ratio plots

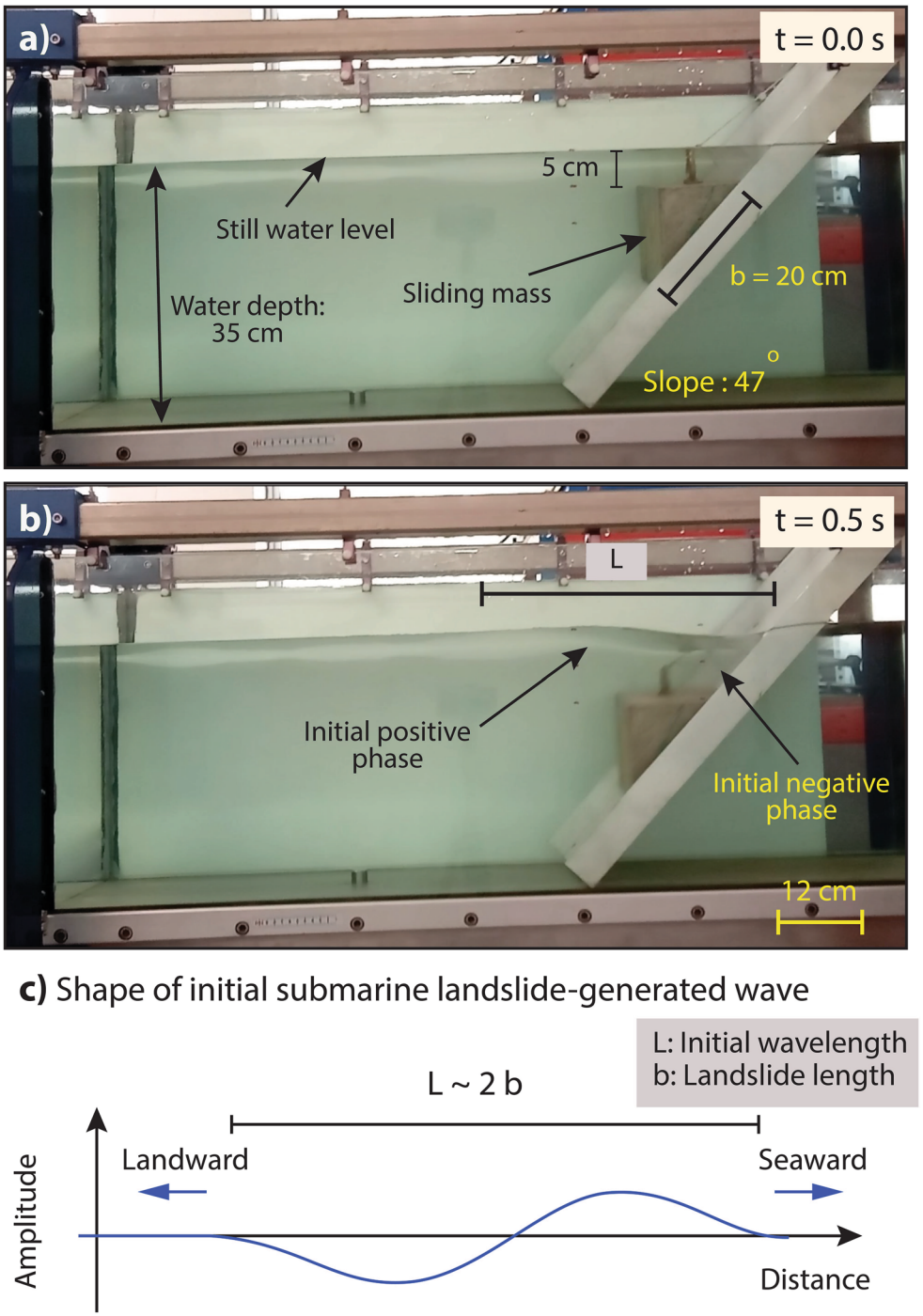

Fig. 4 **a**, **b** Snapshot of a submarine landslide physical experiment at rest (i.e., $t = 0$) and 0.5 s after landslide onset showing generation of an initial negative (depression) phase shoreward and an initial positive (elevation) phase seaward of the landslide. **c** Sketch showing the shape of the initial wave generated by a submarine landslide. "*L*" is the initial surface water displacement, and "*b*" is the length of the landslide as shown in panel a

(e.g., Rabinovich 1997; Heidarzadeh and Satake 2017; Zaytsev et al. 2021; Heidarzadeh et al. 2022a; Wang et al. 2023). Based on the peak periods in Arsuz and Erdemli, we could establish three dominant tsunami period bands of 5.4–7 min, 12–13 min, and 17–21 min (Fig. 5a). Wavelet analyses reveal that the period bands of 12–13 min, and 17–21 min are more persistent and stronger in Arsuz than in Erdemli (Fig. 5b). On the

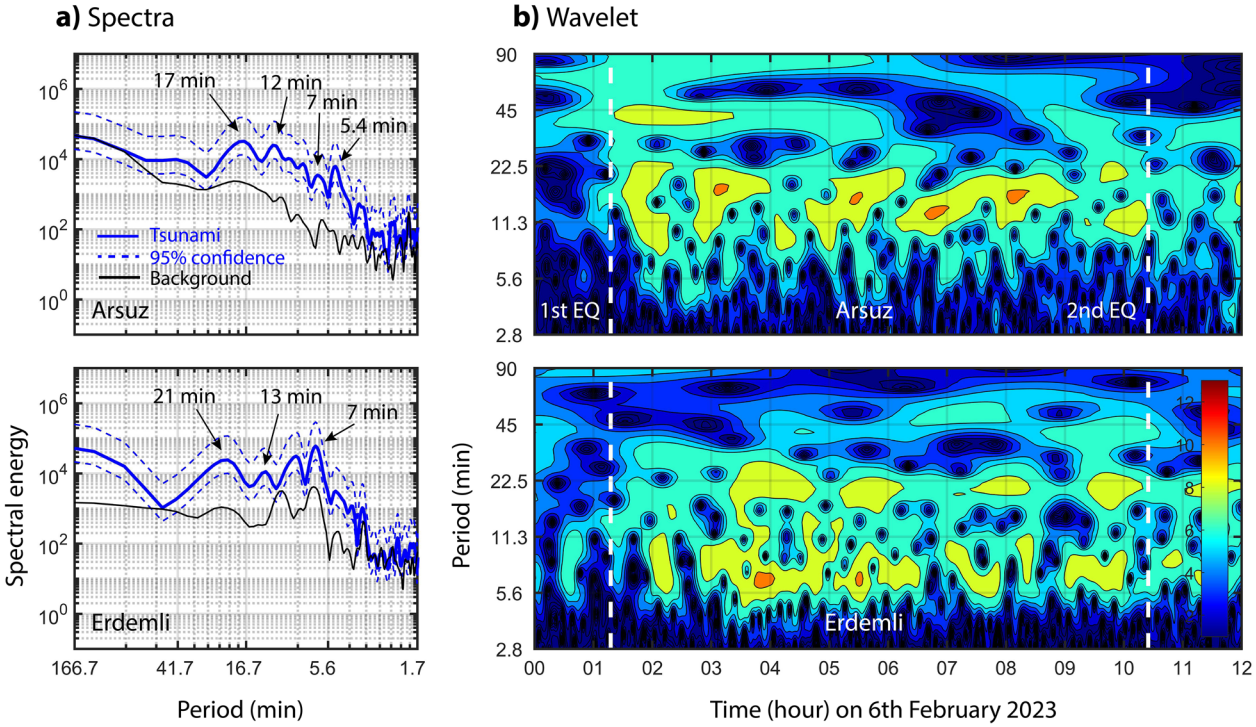

Fig. 5 Spectra **a** and wavelet **b** plots for the tide gauge records of the 6th February 2023 eastern Mediterranean tsunami. Here, 1st EQ and 2nd EQ refer to the two earthquakes on 6th February 2023 at 01:17:35 UTC (M_w 7.8) and 10:24:49 UTC (M_w 7.5), respectively (see Fig. 1 for their locations)

other hand, the period band of 5.4–7 min is stronger in Erdemli than in Arsuz. Wavelet plots reveal distinct tsunami oscillations patterns between Arsuz and Erdemli: while most of the tsunami energy is channeled to the period band of 12–13 min and 17–21 min in Arsuz, two evident channels of 7 min and 21 min are seen in the wavelet plot of Erdemli. This may indicate that the tsunami wavefield was more complicated in Erdemli than in Arsuz.

The peak tsunami periods (T_p) can be used to estimate the characteristic length of the initial sea surface displacement of a tsunami (L), for example, using the following equation (Heidarzadeh and Satake 2015):

$$L = \frac{T_p}{2}\sqrt{gd} \tag{2}$$

where, L is the characteristic length (or width) of the initial surface water displacement generated by a submarine landslide, T_p is peak tsunami period, g is gravitational acceleration, and d is water depth around the source region. Considering the water depths of $d = 100$–200 m (150 m as average) for the source region (Fig. 1), and the peak periods (T_p) of 5.4–7 min (6.2 min as average), 12–1 min (12.5 min as average), and 17–21 min (19 min as average), we estimate the characteristic length of the initial surface water displacement to be approximately in the range of 5 – 28 km for these period bands.

Modelling tsunamis from the earthquake source

We applied the earthquake source model of the USGS as the initial source of the tsunami and modelled its propagation (Fig. 6). Simulation results reveal that the modeled tsunami is negligible and the maximum simulated amplitude at the closest tide gauge to the epicenter (Arsuz) is around 2 cm, whereas observed tsunami has a maximum amplitude of 15.2 cm in Arsuz (Table 1). In addition, the simulated waves show longer wave periods compared to the observations. For the other two stations of Erdemli and Tasucu, it can be seen that the simulated tsunami waveforms are less than 1 cm and bear no resemblance to the observed waveforms. Therefore, there is no doubt that the crustal deformation from the earthquake cannot be considered as the source of the tsunami observed in these stations. In other words, it is likely that a secondary source, triggered by the earthquake, was responsible for the generation of the tsunami. The most plausible secondary source can be a submarine landslide.

Normally submarine landslides generate short-period tsunamis as compared to earthquakes due to the relatively smaller sizes of submarine landslides (Synolakis 2003; Heidarzadeh et al. 2014; Takagi et al. 2019). The

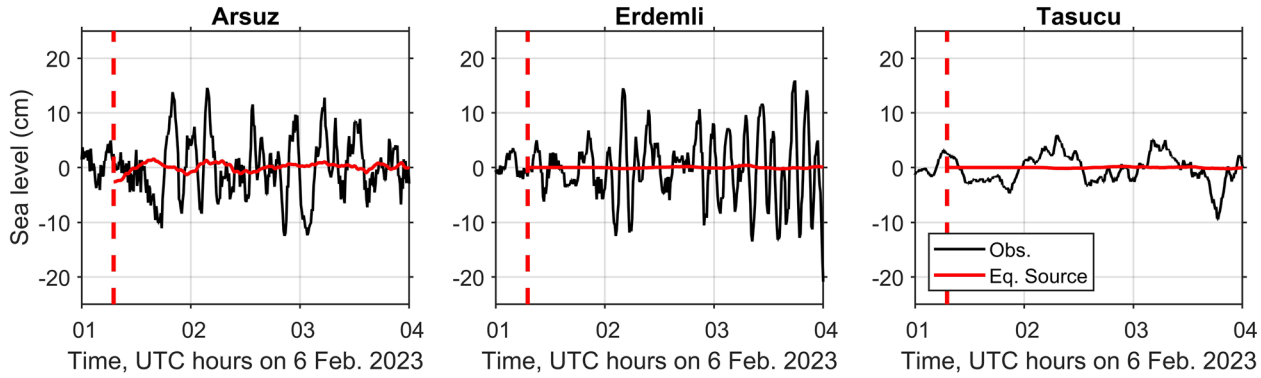

Fig. 6 Results of tsunami simulations (red waveforms) by considering the earthquake (M_w 7.8) as the source of the tsunami. The "Eq. source" refers to the USGS source model (see Fig. 3). The black waveforms show tsunami observations. The red vertical dashed line represents the origin time of the first earthquake (M_w 7.8)

fact that the observed tsunami on 6th February 2023 shows shorter periods compared to the simulated waves from the earthquake source (Fig. 6) may strengthen our hypothesis that the February 2023 tsunami was produced by a submarine landslide or landslides.

Backward tsunami travel time mapping

Backward tsunami travel time mapping is based on considering hypothetical tsunami sources at the location of a tsunami observation station (e.g., a tide gauge) and allowing the waves to propagate backward from that station to the open sea for the amount of actual tsunami travel times (TTT) of that station. This will produce a reverse (or backward) tsunami travel time contour. The zone where all reverse travel time contours from all stations meet is considered as the source of the tsunami. Backward tsunami travel time mapping is a powerful tool for pinpointing the location of tsunami source, and thus has been used in the past for both tectonic and landslide tsunamis. For example, Hayashi et al. (2011) and Mulia and Asano (2016) applied this technique to constrain the extension of the earthquake source of the March 2011 Japan tsunami due to the M_w 9.0 off-Tohoku earthquake. Heidarzadeh and Satake (2014) employed this method to identify the location of the submarine landslide responsible for the September 2013 tsunami following M_w 7.7 Pakistan inland earthquake. Heidarzadeh et al. (2022b) applied this method on the 16 June 2021 Seram Island (Indonesia) tsunami.

For the case of the 6th February 2023 tsunami, the TTT for each tide gauge station is given in Table 1 and shown in Fig. 2. The outcome of backward tsunami travel time mapping is presented in Fig. 7. Various uncertainties are associated with this analysis including those arising from bathymetry data and TTT estimates. For example, considering that the area of the tsunami is shallow with water depth of 100–200 m, a 30 m error in bathymetry data results in an error of approximately 11 km for the location of the tsunami source. Also, an error of 4 min for estimating TTT would result in a dislocation of approximately 9 km for the tsunami source. In addition, a point source is considered for backward travel time mapping while actual tsunami source is not a point source. Therefore, it is natural that the analysis (Fig. 7) gives a zone with length of approximately 45 km as the potential area of the tsunami source. It is noted that the boundaries of the tsunami source region (dashed box in Fig. 7) are not definitive, and we consider an uncertainty zone of at least ± 11 km. Despite such uncertainties, it is believed that the potential landslide zone obtained by backward tsunami travel time mapping is a success, and is helpful towards identifying the source of the tsunami.

As the co-seismic crustal deformation was far from the coastal area (Fig. 3), it is most likely that the tsunami was produced by a submarine landslide that occurred in the area marked in Fig. 7. Another evidence that further supports this hypothesis is that the observed tsunami waves show shorter periods as compared to the simulated waves from the earthquake source (see Fig. 6). We test the hypothesis of a landslide being the source of the tsunami by performing full numerical modelling of tsunamis from potential submarine landslides.

Modelling tsunami from potential landslide sources

In this section, we apply an iterative trial-and-error approach by numerical modelling of landslide source candidates to identify the most credible landslide source. By considering the landslide zone identified by backward tsunami travel time mapping (Fig. 7) and estimates of the sizes of the initial water displacement, we considered seven candidate submarine landslide sources (LS)

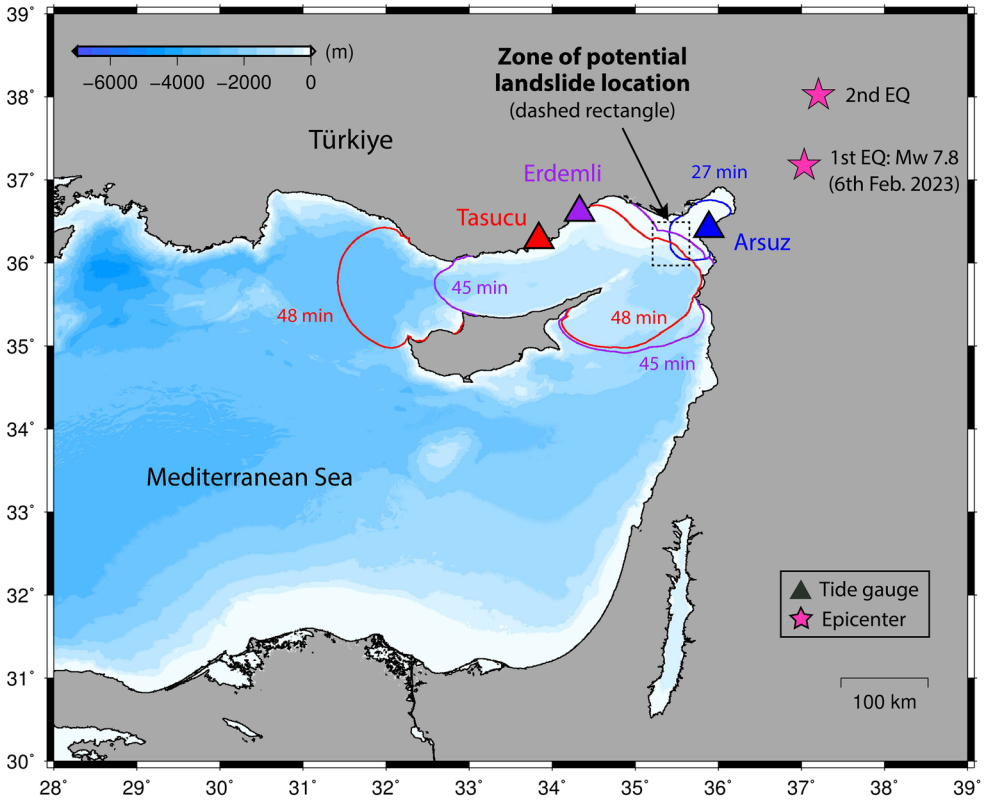

Fig. 7 Backward tsunami travel time mapping for the 6th February 2023 eastern Mediterranean tsunami using the records of three tide gauges that registered tsunami signals (Arsuz, Erdemli, and Tasucu)

located in and around the zone (Fig. 8, Table 3). The source scenarios have maximum positive initial amplitudes of 0.5 m–2.0 m and maximum negative initial amplitudes of 0.6 m – 2.8 m (Table 3). The lengths and widths of the initial sea surface displacements for these LS scenarios range in the domains of 18.0 km–32.0 km and 8.0 km–8.5 km, respectively (Table 3, Fig. 8). The scenarios are located within or around the potential landslide zone detected by backward tsunami travel time mapping (Fig. 8). To consider the uncertainties associated with backward tsunami travel time mapping, some of the LS scenarios are placed around the borders of the zone (Fig. 8). The volume estimates of the landslide scenarios in Table 3 are based on the volumes of the total displaced water multiplied by two. The rational for applying a factor of two is that the displaced water by each landslide scenario is assumed to be half of the volume of the landslides.

Figures 9, 10 present the results of numerical modelling of tsunamis generated by all seven LS scenarios by comparing the simulated waveforms with observations. LS1, LS2 and LS4 successfully reproduce the initial depression wave observed in Arsuz, but the simulated initial waves arrive earlier, and the amplitudes of the simulated waves are much larger than the observations. Another major problem is that all these three scenarios (LS1, LS2, LS4) produce short-period waves as compared to the observations. LS3 gives good results in Arsuz in terms of both amplitudes and arrival times, and the results are acceptable in Erdemli only for the first wave (Fig. 9). A good agreement between the period of the simulated and observed waves is seen for LS3, which is considered as an advantage of LS3 over the previous three scenarios. LS5 overestimates the waves both in Arsuz and Erdemli and the periods of the simulated waves are noticeably shorter than the observations (Fig. 10). The last two scenarios, LS6 and LS7, appear to underestimate the waves and produce short-period waves as compared to observations.

In summary, simulations reveal that LS3 is the best scenario among the examined ones and can reproduce the amplitudes and periods of the observations reasonably well.

The most credible landslide tsunami source and discussions

The final best-fit source model (model LS3; Fig. 11) can well reproduce the tsunami observations. In terms of waveform spectra, a relatively good agreement is seen

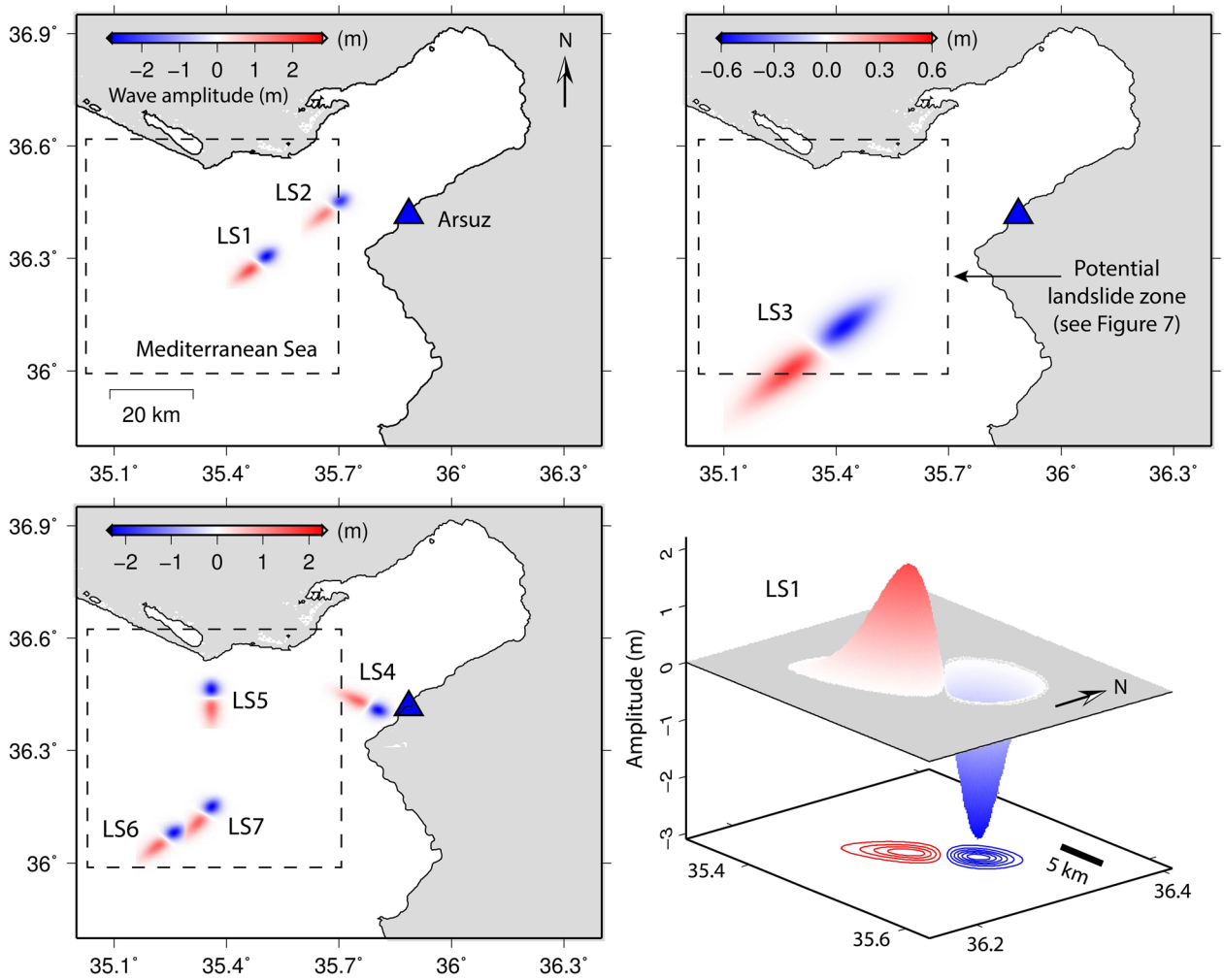

Fig. 8 All submarine landslide (LS) alternative source scenarios considered in this study. The dashed box shows the potential landslide zone identified by backward tsunami travel time mapping (see Fig. 7)

Table 3 Seven candidate submarine landslide scenarios considered in this study to model the 6th February 2023 eastern Mediterranean tsunami

Scenario name	Longitude (°)	Latitude (°)	Length/width of initial water displacement (km/km)	Maximum positive phase (m)	Maximum negative phase (m)	Landslide volume (km^3)
LS1	35.50	36.30	20/8.5	2.0	− 2.8	0.19
LS2	35.70	36.45	18/8.0	1.4	− 2.3	0.14
LS3	35.40	36.10	32/8.5	0.5	− 0.6	0.25
LS4	35.80	36.41	18/8.0	1.4	− 2.3	0.14
LS5	35.36	36.46	18/8.0	1.4	− 2.3	0.14
LS6	35.26	36.08	18/8.0	1.4	− 2.3	0.14
LS7	35.36	36.15	18/8.0	1.4	− 2.3	0.14

For calculating the length and width of the candidate sources, the area within the minimum absolute amplitude of 3–4 cm is considered. The volume estimates of the landslide scenarios are based on the volumes of the total displaced water multiplied by two

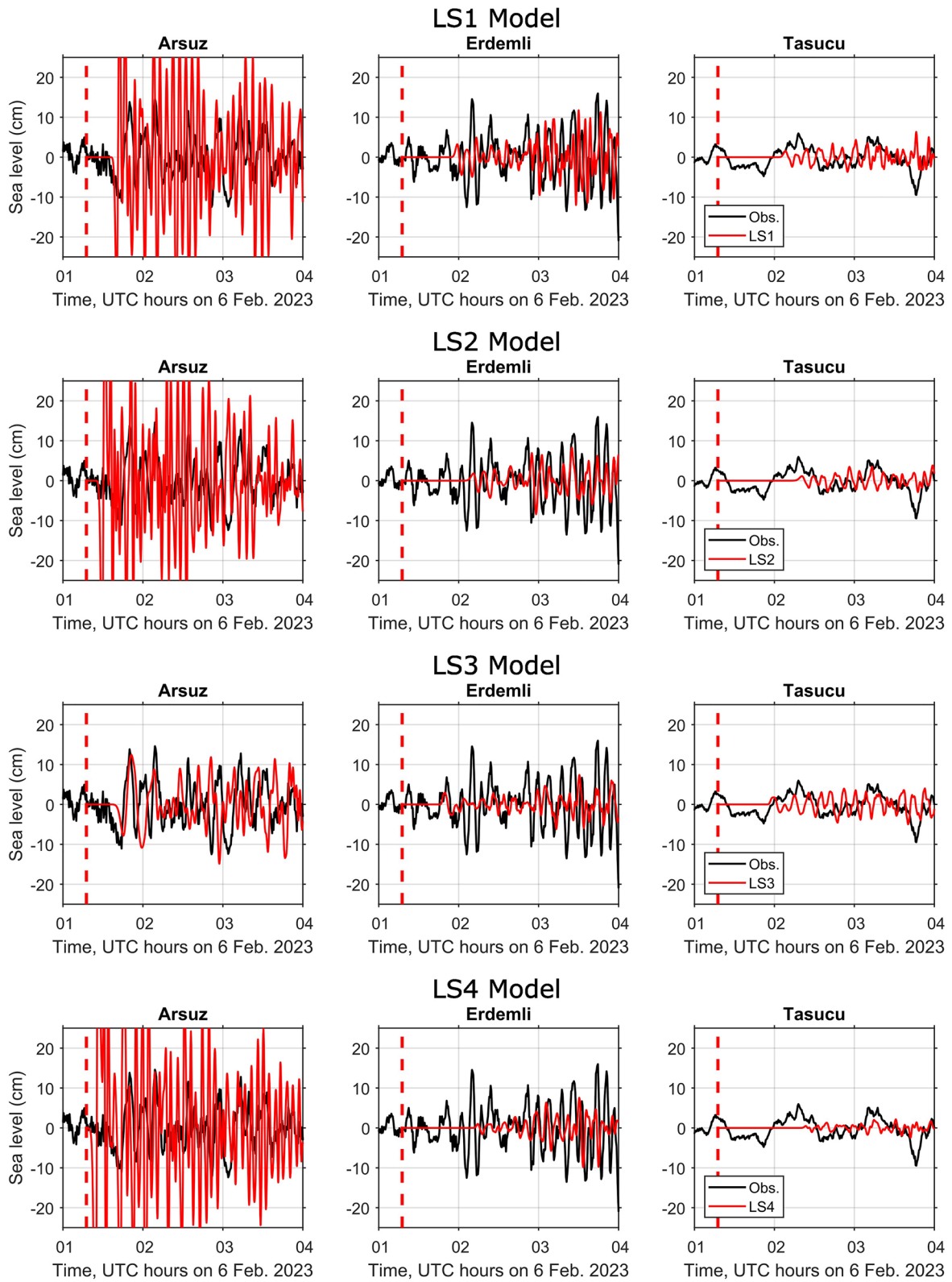

Fig. 9 Results of tsunami simulations (red waveforms) from hypothetical submarine landslide scenarios LS1–LS4. The black waveforms show tsunami observations at various tide gauges. The vertical dashed line represents the origin time of the first earthquake (M_w 7.8)

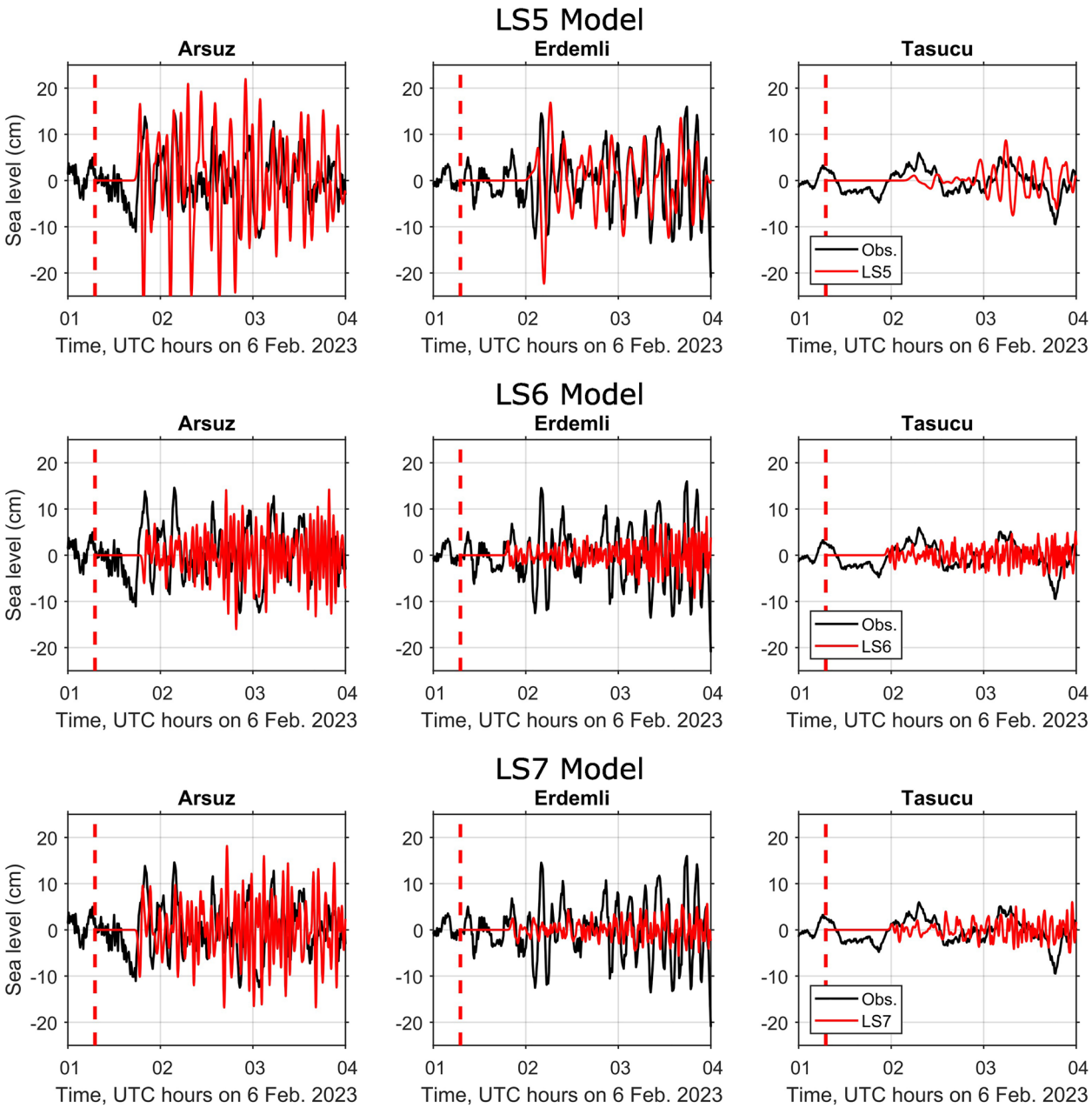

Fig. 10 Results of tsunami simulations (red waveforms) from hypothetical submarine landslide scenarios LS5–LS7. The black waveforms show tsunami observations at various tide gauges. The vertical dashed line represents the origin time of the first earthquake (M_w 7.8)

between the spectra of the observations and simulations based on the final best-fit source model (Fig. 12). Applying Relationship (1), and by considering that the initial water surface displacement due to LS3 was 32 km × 8.5 km (Table 3), we estimate the size of the submarine landslide LS3 on the seafloor to be approximately 16 km (length) × 4 km (width).

As for limitations of this study, it is worth noting that our final best-fit source model (Fig. 11) is exclusively based on waveform analyses and numerical modelling, and it is not confirmed by geological mapping of the seafloor. The bathymetry data used in this study (i.e., GEBCO) is known as being uncertain in shallow water around the coastal areas and thus is not suitable for such geological studies. Despite this, it is helpful noting that our final best-fit source model is located on a relatively steep slope on a transition zone on the seafloor where water depth rapidly changes from 200 m to over 800 m.

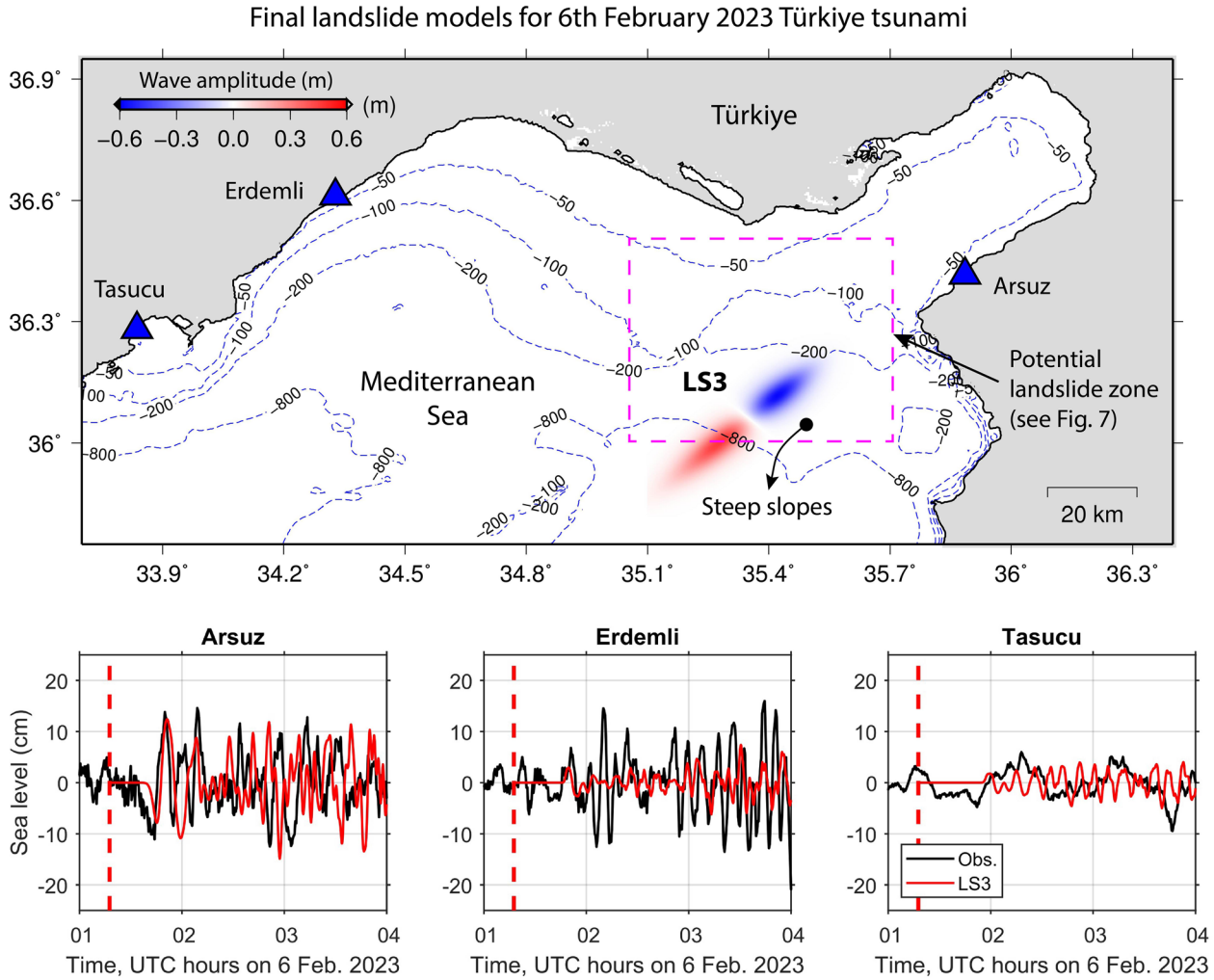

Fig. 11 The final submarine landslide best-fit source model (LS3) for the 6 February 2023 eastern Mediterranean tsunami following the M_w 7.8 inland Türkiye–Syria earthquake. The blue dashed contours at the top panel show bathymetry contours in meters. The red vertical dashed lines at the bottom panels represent the origin time of the first earthquake

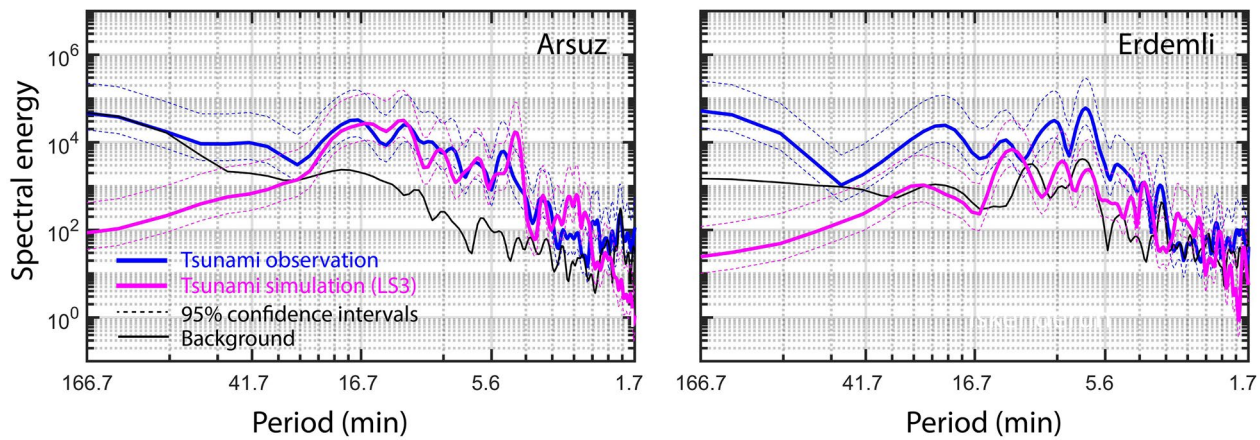

Fig. 12 Comparison of Fourier analyses of the observed (blue) and simulated (pink) waveforms for the final best-fit source model (LS3). The black spectra show background signals using the tsunami observation waveforms

As marine geological surveys are expensive and time-consuming, our results offer precious information regarding the location of submarine landslides, and thus can be used as guides in future marine geophysical surveys to save time and costs. The other limitation of this study concerns the quality of the bathymetric data, which is based on the GEBCO digital atlas and is not generally considered as high-resolution bathymetry data. It is recommended that potential future bathymetric surveys of the area produce high-resolution bathymetry data. There is no concrete and universal relationship to relate the size of the initial water surface displacement of a tsunami to the dimension of the seafloor deformation of a landslide. Our proposed relationship (1) should be considered as a rule of thumb.

It may be helpful noting that landslides may generate some seismic waves that could be recorded on seismic stations. The clarity of such signals among many other signals from the mainshock and aftershocks depends on the size and speed of the landslide and the distance of the seismic stations to the landslide location. In general, such seismic signals from landslides are hidden among other signals and our previous efforts for identifying them for the September 2013 offshore Pakistan event (Heidarzadeh and Satake 2014) was unsuccessful. Nevertheless, we recommend looking at such signals for future studies.

Conclusions

It has been a puzzle as how the 6th February 2023 East Mediterranean tsunami was generated following the M_w 7.8 Türkiye–Syria earthquake considering that the epicenter was approximately 90 km inland. We developed a novel hybrid methodology for the first time and applied it here to solve this puzzle and showed that the tsunami was generated by a submarine landslide triggered by the earthquake. Our hybrid methodology employs a combination of waveform, spectral, and backward tsunami travel time mapping analyses as well as numerical modeling. Main findings are:

- Three dominant tsunami period bands were identified through spectral analyses of the tide gauge waveforms, which are: 5.4–7 min, 12–13 min, and 17–21 min. Based on these dominant tsunami period bands, the dimension of the initial water surface displacement of the tsunami is approximated in the range of 5–28 km. This theoretical dimension guided us to decide the dimensions of the candidate tsunami sources.
- Tsunami simulations based on the earthquake source (M_w 7.8) revealed that the simulated tsunami was too small compared to the observations, and thus the coseismic crustal deformation of the earthquake was ruled out as the tsunami source.
- The tsunami was most likely generated by a submarine landslide and the location of the landslide was constrained using backward tsunami travel time mapping. A zone was given by backward tsunami travel time mapping for the location of the potential submarine landslide.
- By considering seven candidate landslide sources and conducting numerical modelling, we were able to reproduce the observed tsunami using one of the submarine landslide scenarios reasonably well. It is located on a steep slope of the seafloor approximately 50 km from Arsuz. The submarine landslide is estimated to have caused a seafloor deformation measuring approximately 16 km in length and 4.0 km in width.

Acknowledgements
Some figures were drafted using the GMT mapping tool (Wessel and Smith 1998). We acknowledge the University of Bath Institutional Open Access Fund. A. R. Gusman was supported by the New Zealand Ministry for Business, Innovation, and Employment (MBIE) through the Strategic Science Investment Fund (SSIF) and the Rapid Characterization of Earthquakes and Tsunami: Fewer deaths and faster recovery project (Endeavour fund). We are grateful to Prof Kenji Satake (Editor-in-Chief) and Dr Anawat Suppasri (Editor) for their helpful comments. The manuscript benefited from constructive review comments from two anonymous reviewers for which we are grateful.

Author contributions
MH developed the idea, conducted sea level data and spectral analyses, and drafted the manuscript. ARG conducted numerical modelling and wrote the associated parts. IEM prepared the earthquake source model. All co-authors read and commented on the manuscript.

Funding
This study is supported by the Great Britain Sasakawa Foundation grant no. 6217 (awarded in 2023). We acknowledge the University of Bath Institutional Open Access Fund.

Availability of data and materials
The bathymetric data are from the GEBCO digital atlas (https:// www.gebco.net/). Tide gauge data are provided by Intergovernmental Oceanographic Commission's sea level station monitoring facility (http://www.ioc-sealevelmonitoring.org/map.php). The USGS earthquake source model can be found here: https://earthquake.usgs.gov/earthquakes/eventpage/us6000jllz/finite-fault. Other data can be provided by writing to the corresponding author.

Declarations

Competing interests
All authors declare that there are no competing interests.

Author details
[1]Department of Architecture and Civil Engineering, University of Bath, Bath BA2 7AY, UK. [2]GNS Science, 1 Fairway Drive, Avalon, Lower Hutt 5010, New Zealand. [3]Prediction Science Laboratory, RIKEN Cluster for Pioneering Research, 7-1-26 Minatojima-minami-machi, Chuo-ku, Kobe 650-0047, Japan. [4]Disaster Resilience Science Team, RIKEN Center for Advanced Intelligence Project, 1-4-1 Nihonbashi, Chuo-ku, Tokyo 103-0027, Japan.

Received: 2 May 2023 Accepted: 10 October 2023
Published online: 20 October 2023

References

Barka A (1999) The 17 august 1999 Izmit earthquake. Science 285(5435):1858–1859

Cheng AC, Suppasri A, Pakoksung K et al (2023a) Resonance characteristics and impact of the 2006 Pingtung tsunami in southern Taiwan. Geosci Lett 10:17. https://doi.org/10.1186/s40562-023-00271-0

Cheng AC, Suppasri A, Pakoksung K, Imamura F (2023b) Characteristics of consecutive tsunamis and resulting tsunami behaviors in southern Taiwan induced by the Hengchun earthquake doublet on 26 December 2006. Nat Hazards Earth Sys Sci 23(2):447–479

Dogan GG, Annunziato A, Papadopoulos GA, Guler HG, Yalciner AC, Cakir TE, Synolakis C et al (2019) The 20th July 2017 Bodrum-Kos tsunami field survey. Pure Appl Geophys 176:2925–2949

Dogan GG, Yalciner AC, Yuksel Y, Ulutaş E, Polat O, Güler I, Kânoğlu U et al (2021) The 30 October 2020 Aegean Sea tsunami: post-event field survey along Turkish coast. Pure Appl Geophys 178:785–812

GEBCO Compilation Group (2022) GEBCO_2022 Grid. https://https://doi.org/10.5285/e0f0bb80-ab44-2739-e053-6c86abc0289c.

Grilli ST, Watts P (2005) Tsunami generation by submarine mass failure I: modeling, experimental validation, and sensitivity analyses. J Waterway Port Coast Ocean Eng 131(6):283–297

Grinsted A (2023) Tidal fitting toolbox (https://www.mathworks.com/matlabcentral/fileexchange/19099-tidal-fitting-toolbox). MATLAB Central File Exchange. Retrieved 27 Mar, 2023.

Hayashi Y, Tsushima H, Hirata K, Kimura K, Maeda K (2011) Tsunami source area of the 2011 off the Pacific coast of Tohoku Earthquake determined from tsunami arrival times at offshore observation stations. Earth Planets Space 63:809–813

Heidarzadeh M, Gusman AR (2021) Source modeling and spectral analysis of the crete tsunami of 2 May 2020 along the Hellenic Subduction Zone, offshore Greece. Earth Planets Space 73:74. https://doi.org/10.1186/s40623-021-01394-4

Heidarzadeh M, Satake K (2014) Possible sources of the tsunami observed in the northwestern indian ocean following the 2013 September 24 Mw 77 Pakistan inland earthquake. Geophys J Int 199(2):752–766. https://doi.org/10.1093/gji/ggu297

Heidarzadeh M, Satake K (2015) New Insights into the Source of the Makran Tsunami of 27 November 1945 from Tsunami Waveforms and Coastal Deformation Data. Pure Appl Geophys 172(3):621–640. https://doi.org/10.1007/s00024-014-0948-y

Heidarzadeh M, Satake K (2017) Possible dual earthquake–landslide source of the 13 November 2016 Kaikoura. New Zealand Tsunami Pure Appl Geophys 174(10):3737–3749. https://doi.org/10.1007/s00024-017-1637-4

Heidarzadeh M, Krastel S, Yalciner AC (2014) The State-of-the-art numerical tools for modeling landslide tsunamis: a short review submarine mass movements and their consequences, chapter 43. Springer International publishing, Berlin

Heidarzadeh M, Harada T, Satake K, Ishibe T, Takagawa T (2017) Tsunamis from strike-slip earthquakes in the Wharton Basin, northeast Indian Ocean: March 2016 M w7.8 event and its relationship with the April 2012 M w 8.6 event. Geophys J Int 211(3):1601–1612. https://doi.org/10.1093/gji/ggx395

Heidarzadeh M, Necmioglu O, Ishibe T, Yalciner AC (2017a) Bodrum-Kos (Türkiye-Greece) Mw 66 earthquake and tsunami of 20 2017 a test for the Mediterranean tsunami warning system. Geosci Lett 4:31. https://doi.org/10.1186/s40562-017-0097-0

Heidarzadeh M, Murotani S, Satake K, Takagawa T, Saito T (2017c) Fault size and depth extent of the Ecuador earthquake (Mw78) of 16 April from teleseismic and tsunami data. Geophys Res Lett 44(5):2211–2219

Heidarzadeh M, Tappin DR, Ishibe T (2019) Modeling the large runup along a narrow segment of the Kaikoura coast, New Zealand following the November 2016 tsunami from a potential landslide. Ocean Eng 175:113–121. https://doi.org/10.1016/j.oceaneng.2019.02.024

Heidarzadeh M, Pranantyo IR, Okuwaki R, Dogan GG, Yalciner AC (2021) Long tsunami oscillations following the 30 October 2020 Mw 7.0 aegean sea earthquake: observations and modelling. Pure Appl Geophys 178:1531–1548. https://doi.org/10.1007/s00024-021-02761-8

Heidarzadeh M, Gusman A, Ishibe T, Sabeti R, Šepić J (2022a) Estimating the eruption-induced water displacement source of the 15 January 2022 Tonga volcanic tsunami from tsunami spectra and numerical modelling. Ocean Eng 261:112165. https://doi.org/10.1016/j.oceaneng.2022.112165

Heidarzadeh M, Gusman AR, Patria A, Widyantoro BT (2022) Potential landslide origin of the Seram Island tsunami in Eastern Indonesia on 16 June 2021 following an Mw 5.9 earthquake. Bull Seismol Soc Am 112(5):2487–2498. https://doi.org/10.1785/0120210274

Hu G, Satake K, Li L, Du P (2023) Origins of the tsunami following the 2023 Turkey-Syria earthquake. Geophys Res Lett 50(18):e2023GL103997

International Medical Corps (2023) Syria/Türkiye Earthquakes Situation Report #7. March 8, 2023. Situation Report. https://reliefweb.int/report/syrian-arab-republic/syriaTürkiye-earthquakes-situation-report-7-march-8-2023

Liu PLF, Woo SB, Cho YS (1998) Computer programs for tsunami propagation and inundation. Cornell University, USA

Mathworks (2023) MATLAB user manual. MathWorks Inc., Natick

Mulia IE, Asano T (2016) Initial tsunami source estimation by inversion with an intelligent selection of model parameters and time delays. J Geophys Res 121(1):441–456. https://doi.org/10.1002/2015JC010877

Mulia IE, Gusman AR, Heidarzadeh M, Satake K (2022) Sensitivity of tsunami data to the updip extent of the July 2021 Mw 82 Alaska earthquake. Seismol Res Lett 93(4):1992–2003. https://doi.org/10.1785/0220210359

Okal EA, Synolakis CE (2004) Source discriminants for near-field tsunamis. Geophys J Int 158(3):899–912

Ozalaybey S, Ergin M, Aktar M, Tapirdamaz C, Biçmen F, Yörük A (2002) The 1999 Izmit earthquake sequence in Türkiye: seismological and tectonic aspects. Bull Seismol Soc Am 92(1):376–386

Papadopoulos GA, Gràcia E, Urgeles R, Sallares V, De Martini PM, Pantosti D et al (2014) Historical and pre-historical tsunamis in the Mediterranean and its connected seas: Geological signatures, generation mechanisms and coastal impacts. Mar Geol 354:81–109. https://doi.org/10.1016/j.margeo.2014.04.014

Rabinovich AB (1997) Spectral analysis of tsunami waves: separation of source and topography effects. J Geophys Res 102(C6):12663–12676

Satake K (2014) Advances in earthquake and tsunami sciences and disaster risk reduction since the 2004 Indian ocean tsunami. Geosci Lett 1(1):1–13. https://doi.org/10.1186/s40562-014-0015-7

Satake K, Tanioka Y (2003) The July 1998 Papua New Guinea earthquake: mechanism and quantification of unusual tsunami generation. Pure Appl Geophys 160:2087–2118

Synolakis CE (2003) Tsunami and seiche. In: Chen WF, Scawthorn C (eds) Earthquake Engineering Handbook. CRC Press, Boca Raton

Synolakis CE, Bardet JP, Borrero JC, Davies HL, Okal EA, Silver EA, Sweet S, Tappin DR (2002) The slump origin of the 1998 Papua New Guinea tsunami. Proc R Soc Lon A 458:763–789

Takagi H, Pratama MB, Kurobe S, Esteban M, Aránguiz R, Ke B (2019) Analysis of generation and arrival time of landslide tsunami to Palu City due to the 2018 Sulawesi earthquake. Landslides 16:983–991

Tanioka Y, Satake K (1996) Tsunami generation by horizontal displacement of ocean bottom. Geophys Res Lett 23(8):861–864

Tappin DR, Watts P, Grilli ST (2008) The Papua New Guinea tsunami of 17 July 1998: anatomy of a catastrophic event. Nat Hazards Earth Sys Sci 8(2):243–266

Tinti S, Armigliato A, Manucci A, Pagnoni G, Zaniboni F, Yalçiner AC, Altinok Y (2006) The generating mechanisms of the August 17, 1999 Izmit bay (Türkiye) tsunami: regional (tectonic) and local (mass instabilities) causes. Mar Geol 225(1–4):311–330

Torrence C, Compo GP (1998) A practical guide to wavelet analysis. Bull Am Meteorol Soc 79(1):61–78

Wang Y, Heidarzadeh M, Satake K, Hu G (2022) Characteristics of two tsunamis generated by successive Mw 7.4 and Mw 8.1 earthquakes in Kermadec Islands on March 4, 2021. Nat Hazards Earth Sys Sci 22:1073–1082. https://doi.org/10.5194/nhess-22-1073-2022

Wang Y, Wang P, Kong H, Wong CS (2023) Tsunamis in Lingding Bay, China, caused by the 2022 Tonga volcanic eruption. Geophys J Int 232(3):2175–2185. https://doi.org/10.1093/gji/ggac291

Wang X, Power WL (2011) COMCOT: a tsunami generation propagation and run-up model. GNS Science.

Wang X (2008) Numerical modelling of surface and internal waves over shallow and intermediate water. Cornell University.

Watts P, Grilli ST, Tappin DR, Fryer GJ (2005) Tsunami generation by submarine mass failure II: predictive equations and case studies. J Waterway Port Coast Ocean Eng 131(6):298–310

Wessel P, Smith WHF (1998) New improved version of generic mapping tools released. EOS Trans Am Geophys Union 79(47):579–579

Yalciner AC, Zaytsev A, Aytore B, Insel I, Heidarzadeh M, Kian R, Imamura F (2014) A possible submarine landslide and associated Tsunami at the Northwest Nile Delta. Mediterranean Sea Oceanogr 27(2):68–75. https://doi.org/10.5670/oceanog.2014.41

Yalciner AC, Synolakis CE, Borrero J, Altinok Y, Watts P, Imamura F, Kuran U, Ersoy S, Kanoglu U, Tinti S (1999) Tsunami generation in Izmit Bay by the Izmit earthquake. In: Proceedings ITU-IAHS International Conference on the Kocaeli Earthquake 17 August 1999, 217–221.

Zaytsev O, Rabinovich AB, Thomson RE (2021) The impact of the chiapas Tsunami of 8 September 2017 on the Coast of Mexico. Part 1: observations, statistics, and energy partitioning. Pure Appl Geophys 178:4291–4323. https://doi.org/10.1007/s00024-021-02893-x

Publisher's Note